

A Spatio-Causal Growth Model Explains the Pareto Principle

Andre F. Ribeiro¹

¹University of Sao Paulo, Sao Carlos, SP, 13560-970, Brazil

Under typical growth models, populations quickly lose the ability to select and sustain effects (gains and losses), as growth leaves their increasing variation (endogenous and exogenous) uncontrolled. Under (1) Unconfounded growth, in contrast, populations preserve the ability to determine which of their variations are responsible for the gains and losses they observe (and can, consequently, carry fair selection and optimization processes). Under (2) Externally-Valid growth, effects generalize across populations' full range of external variation (and populations can, consequently, expand across increasingly diverse conditions). The first promotes generalization of effects over populations, and the second over their environments. These alternative growth patterns allow systems in complex environments to create sustainable environments for growth, from their spatial distribution patterns.

We consider the full growth, from 1840, of American cities and economy. We use billions of individual-level census records, organized in spatial-levels ranging from the street level all the way to the national. We demonstrate populations' combinatorial thresholds for sustainable growth, across locations and levels. The resulting binomial-exponential model unifies popular mathematical growth theories, and reveals new connections to the Fibonacci-Golden ratio, Cooperative Game-Theory, Spatial Experimental-Designs, Causality, Power-laws, Hyperbolic Geometry, and the Pareto Principle. It, finally, makes new predictions about the growth of cities, that are hard to explain with current models.

1 Introduction

Observations of effects in everyday social and biological systems are riddled with statistical problems familiar to any researcher - low effect generalizability, heterogeneity, confounding and selection biases. Commonly studied processes such as Economic and Evolutionary Competition, Epistemic Development and Viral transmission are not immune to any of these. In each case, it is unclear to what extent these statistical pitfalls are simple nuisances, or have a shaping influence in the overall operation of systems. Here, we use recent advances in the understanding of how combinatorial properties of populations constraints learning to address this question.

The **Pareto Principle** states that '80% of consequences come from 20% of the causes', or, that a minority of factors are typically responsible for outcomes¹⁻³. It was devised and observed first across economic outputs, becoming a principle of Welfare Economics and the study of inequality. Today, it is known to be ubiquitous across human processes. The pattern is evident in the

output of cities, corporations, scientists, sport teams, criminals, websites, etc. It is often used as a heuristic in Business and Engineering. In a previous article ⁴, we discussed the related 80-20% train-test split in Machine Learning. **The principle remains, however, a mere fact of observation** and not a scientific theory in any sense. Mathematically, the 80-20 rule is described by a power-law, but for a very particular set of parameters, when its shape is $\log_4 5 = \log_{10} 5 / \log_{10} 4 \approx 1.161$. Why is this ratio so prevalent across selective and competitive systems?

Most empirical mathematical models for the spatial growth of cities, such as Power-law and Levy-flight⁵⁻⁹, are based on limits introduced by physical distances among homogeneous 'particles', and not the demographic ^{10,11} and recombination processes ^{12,13} shaping growth (see *Sect. Related Models*). These models become useful at high agglomerate levels, where they can employ the Law of Large Numbers to explain statistical issues away. As consequence, however, they (1) lose in specificity and predictive accuracy, and, (2) miss the shaping influence population diversity and biases may have in systems' own growth. Understanding the limits and opportunities brought by population heterogeneity is a current challenge across disciplines¹⁴, from precision Medicine to Machine Learning. In spatial systems, in particular, it is not yet clear **how biases evolve with spatial-levels**, and which levels are optimal in respect to each. There have been recurrent graph-theoretical attempts to connect population diversity, or combinatorial structures, with systems performance ^{15,16}. But theories so far have not led to clear empirical confirmation and lack in simplicity (compared to the previous law-like models).

A remarkable characteristic of all previous systems is their ability to create inner-outer boundaries and hierarchies that are capable of coping with increasingly complex environments. To that end, they must satisfy two opposing requirements. Systems must promote robustness across their out-of-control contingencies ¹⁷ and selectability among their under-control¹⁸. We say a System undergo Externally Valid (EV) growth when effects of its internal variations remain general across external. They undergo Unconfounded (CF) growth when internal effects remain distinguishable. Competitive processes are a common example of selective processes, and mechanisms to select solutions with largest comparative fitness in populations.

Counterfactuals and Games. Most game-theoretic solutions, such as the standard Nash equilibrium, are formulated from counterfactuals. These are what-if statements (i.e., what would happen to a player's utility if he or she took action a , but all else remained constant). Fig.1(a, left) shows a Rock-paper-scissor game (3 simulation runs, gray curves). Each player utility depends on a common noise, $\mathcal{N}(0, 0.1)$, that is not observed. Players follow the replicator dynamics ¹⁹, a learning strategy akin to natural selection. The state space depicts the probability of players playing each of the 3 actions (triangle corners). The Nash equilibrium is a cyclic choice among them, which players fail to attain. Imagine, however, that players agree to play the game in two phases. In the first, they forego immediate strategic choices to accumulate a full set of action counterfactuals. Fig.1(a, right) shows the state space in this alternative scenario, where trajectories coincide with the theoretic equilibrium, across runs. Players play cooperatively to a combinatorial threshold, and

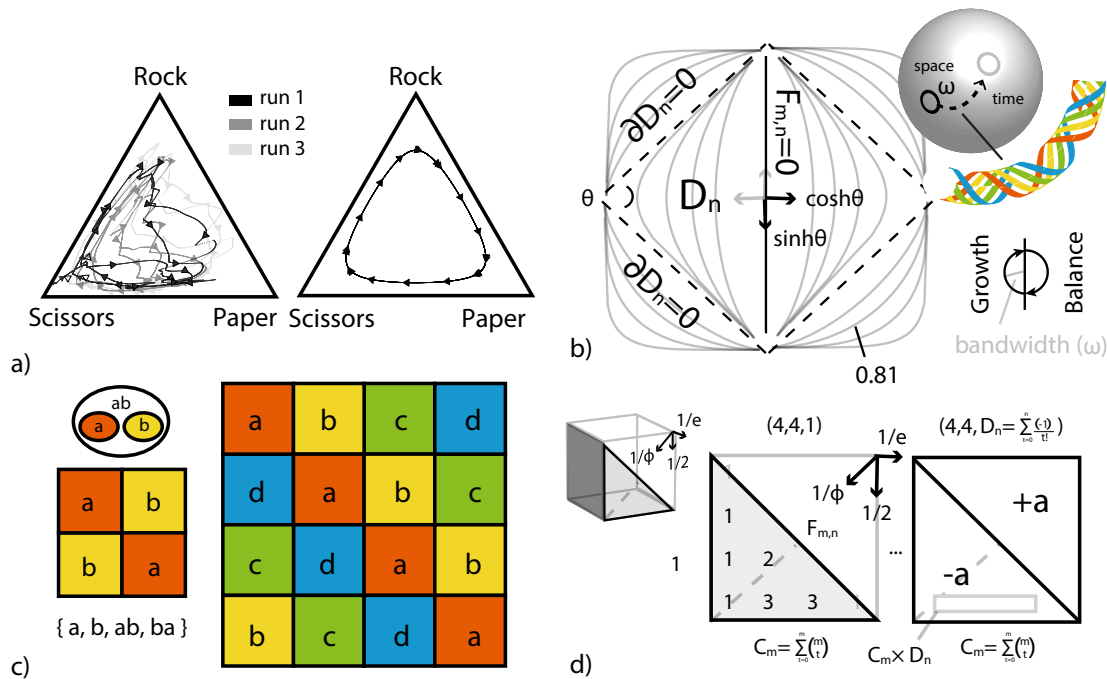


Figure 1: **(a)** Rock-Paper-Scissor game simulation under replicator dynamics with a small exogenous noise (left, 3 runs), after accumulation of a complete set of counterfactual utility observations (right), **(b)** Can counterfactual effect observations made in one location be used in another (are they externally valid, EV)? Can they be distinguished from others (are they unconfounded, CF)?, reciprocal growth and balance phases and their representation as hyperbolic rotations, the first increases the number of external conditions effects are measured under (EV), the second of internal conditions (CF), each have distinct statistical consequences on growing populations, **(c)** a $m \times m$ Latin-Square ('square') portrays the full set of counterfactual effect observations with m factors ($m = 2, 4$), further counterfactuals increases guarantees over the generalizability and bias of populations' effect observations, the square's 1st column ($m = 2$, left) is associated with all differences from a reference population x_0 of size 1 (and overlap $m - 1$), $\{a\}$ and $\{b\}$, the 2nd column with differences of size 2 (and zero overlap), $\{a, b\}$, difference-of-differences enumerate all factor permutations, ($\{\{a, b\} - \{a\}\} \sim ba$) and ($\{\{a, b\} - \{b\}\} \sim ab$) (upper-left, nested sets), these *derangements* (permutations without overlaps) are the squares' rows and columns (right), **(d)** Binomial ($\frac{1}{2}$), Fibonacciian ($\frac{1}{\phi}$) and Exponential ($\frac{1}{e}$) rates across squares lead to the hyperbolic relations in (b), each square's triangle area (gray) is related to EV, their area difference to CF, triangle altitude (dashed) to growth 'bandwidth' (number of populations growing under shared EV-CF conditions).

playing-field with minimal statistical guarantees,* before entering competitive play.

2 Model Summary

Statistical Growth with selection can be seen as the enumeration, and evaluation, of counterfactual populations across time. Each population member's growth trajectory is an incremental, and temporally ordered, observation of the value of gaining, or losing, a factor from the m possible, $X = \{a, b, c, \dots, [m]\}$. Each member's trajectory is, however, just one in the $m! \times 2^m$ possible (all factor permutations times gain/loss of each). We say a set of ω simultaneous trajectories, and permutations, leads, instead, to growth with 'bandwidth' ω . The larger the bandwidth, and number of accumulated counterfactuals, the more (external) conditions in which effect observations are made, and the more likely effects are to generalize across unseen conditions. When ω is small, effect generalization is only possible at the cost of long time periods, Fig.1(b, upper-right).

We demonstrate this implies that growth goes through **reciprocal phases of growth and balance** of ω populations. The first permutes ('shuffles'), and the second keeps ('balances') specific frequency relations among new permutations. Together, they maintain basic statistical guarantees across *all* counterfactual interactions and observations, for the ω populations. Growth and balance are in many ways opposites, as growth bias populations. For the replicator equation in Fig.1(a), populations grow monotonically across a selected dimension, and they are only guaranteed to be balanced once. We say this process has unitary bandwidth, $\omega = 1$. Unbiased growth can be understood, combinatorially, in relation to Experimental Designs and, geometrically, to Hyperbolic geometry. The hyperbolic plane's radial component will be associated with the number of permutations accumulated in populations, and the angular component to their balance, Fig.1(b). This portrays growth as rotate-and-forward cycles, in contrast to the forward-only movement of typical processes. We demonstrate empirical patterns in the simultaneous growth of cities, using these representations.

Combinations, Permutations and Partial Permutations. The set of all counterfactuals accumulated by growth at one instant can be visualized with a Latin-Square ('square'). A square, as defined here, is a collection of all differences from a reference population x_0 , $x_0 - \mathcal{P}(X)$, where $\mathcal{P}(X)$ is the set of all subsets of X . It is thus a full set of effect observations. This is illustrated for two factors, $\{a, b\}$, in Fig.1(c, left). The simultaneous presence of populations $x_0 + \{a\}$, $x_0 + \{b\}$ and $x_0 + \{a, b\}$ (e.g., in the same location) allow for all permutations of $\{a, b\}$ be enumerated, and therefore each factor's effect, $\Delta y(a)$, be observed, across full variation of others. Squares represent mathematical groups⁴ (*Sect. Statistical Frame-of-Reference Invariance*). Linear-Algebra and Group-theoretic alternative formulations are discussed in the Supplementary Material.

The statistical concept of 'population' is often associated with combinatorial combinations,

*the threshold can be either enforced by the statistical consequences of play (i.e., by mechanism design), or anticipated by agents with foresight.

as the set of sample units with a given combination of attributes (e.g., high-income white males). There are thus $\binom{m}{t} = \frac{m!}{t!(m-t)!}$ possible populations of size t . A problem with this definition is that it leaves unspecified all non-population factors. To **define a population we, instead, imagine that we fix the t population factors and vary (i.e., permute) all non-population ('external') factors.** This leads to a combinatorial structure known as a partial permutation.

The number of partial permutations with t elements fixed is $\binom{m}{t} \times D_{m-t}$, where D_{m-t} is the number of derangements of size $n = m-t$, $D_{m-t} = \sum_{k=0}^{m-t} \frac{(-1)^k}{k!}$. A derangement is a permutation without overlaps. To specify a population, we thus first fix t factors (combination) then vary the all rest (derangement). Squares are related to the first, and sets of squares to the latter (derangements of combinations)⁴. The full set of permutations, and thus all growth trajectories, can be formulated as sets of partial permutations,

$$m! = \sum_{t=0}^m \binom{m}{t} \times D_{m-t} = \left[\sum_{t=0}^m \frac{(-1)^t m^t}{t!} \right] \times [(m+1)! - 1] \quad (1)$$

$$= \left[\cosh(m-1) + \sinh(m-1) \right] \times (m-1)! + 1. \quad (2)$$

According to Eq.(1, left), the number of differences necessary to collect one square is $\sum_{t=0}^m \binom{m}{t}$, and all squares is $\sum_{t=0}^m \binom{m}{t} D_{m-t}$ (without repetition). With the latter, we also collect all permutations. After the first square, it thus suffices to continuously derange its constituent combinations. The number n of squares, of size $m \times m$, in a location or sample can thus be specified with the 3D vector (m, m, n) , Fig.1(d, left). The odd and even parts of Taylor's expansion of Eq.(1) leads to hyperbolic trigonometric functions, Eq.(2) (Supporting Material). They indicate the 'period' in which full sets of permutations are collected. Hyperbolic trigonometry will be used below as alternative to Lorentz curves in the study of inequality.

Externally-Valid (EV) Growth. The classic definition of factorials tells us that, to generate a permutation, we insert a new factor in all $m - 1$ positions of a previous permutation, $m! = m \times (m - 1)!$, and repeat. Each square is associated with one such step, when m is limited, Eq.(2). Each (singleton) population a , defined as before, is represented by a square diagonal, Fig.1(c). Subsequent square rows and columns correspond to a 's points-of-insertion, and permutations of its external factors. This suggests a process where we insert a after varying, in every way, others; after each insertion, we observe the resulting outcome difference, $\Delta y(a)$. An unbiased effect estimate for a is an average across all observations, and constitute an U-Statistic^{4,20}. There are $F_{m,n} = \sum_{t=0}^m \binom{m-t}{t}$ such sequential observations.[†] $F_{m,n}$ is the number of factor fixations after a - i.e., $\binom{m-1}{1} = m-1$ to fix any second factor, then $\binom{m-2}{2}$ to fix a third, etc.

[†]with the convention that $\binom{m-t}{t} = 0$, when $t > m$.

The two previous quantities, C_m and $F_{m,n}$, appear in Pascal's triangle, since a *single* square can be thought as two mirrored triangles, justified to the left, Fig.1(d, middle). The square's upper triangle is the set of all counterfactuals with a , and the lower, without a , Fig.1(d, right). The number of all possible external conditions for a given square cell is a product of its coordinates, $\binom{m}{t} \times n$, Eq.(1). Square 'area' is the integration of all these individual area elements. Square area is related to EV, while balance between its two triangles' areas to CF. Growth bandwidth is defined, at time t , as $\omega = \frac{F_{m,n}(t)}{D_n(t)}$, or, the number of external observations, $F_{m,n}(t)$, per derangement, $D_n(t)$, in samples or populations.

The growth of C_m , D_n and $F_{m,n}$ assume Pythagorean relations[‡] Fig.1(d),

$$\left(\frac{\partial C_m}{\partial D_n}\right)^{-2} + \left(\frac{\partial D_n}{\partial D_n}\right)^{-2} = \left(\frac{\partial F_{m,n}}{\partial D_n}\right)^{-2}, \quad (3a) \quad \left(\frac{\partial C_m}{\partial F_{m,n}} \text{ const.}\right)$$

$$\frac{1}{\sqrt{1 + \left(\frac{\partial D_n}{\partial C_m}\right)^2}} = \omega, \quad (3b) \quad \frac{1}{\sqrt{1 - \omega^{-2}}} = \cosh(\omega^{-1}), \quad (3c) \quad \left(\frac{\partial F_{m,n}}{\partial D_n} = \omega\right)$$

Eq.(3a) suggests the hyperbolic relationship $\partial C_m^2 - \partial F_{m,n}^2 = \partial D_n^2$, and visualization of growth as hyperbolae with increasing radius D_n , Fig.1(b). The figure shows the hyperbolic asymptotes $C_m = F_{m,n}$ and $C_m = -F_{m,n}$ (dashed). They represent populations with constant EV, $\partial D_n = 0$. The figure also shows the asymptotic population (vertical black line) where exactly all members have factor a , $F_{m,n} = 0$. **Under this condition, no estimator, algorithm, or player is able to estimate a 's effect.** It represents the limiting population with minimum EV, while the outward hyperbolae, populations with increasing EV. Growth in this direction follow a Fibonacci series, whose rate is the Golden number. Notice that $\frac{\partial D_n}{\partial C_m} \in [1/2, 1/e]$, as growth can range between purely CF, $\frac{\partial C_m}{\partial m} = 2$, and EV, $\frac{\partial D_n}{\partial n} = 1/e$, Fig.1(d). The latter (i.e., the rate required for derangements) was famously established by Euler²¹, and the former is due to $C_m = 2^m$. The combined binomial-exponential process 'doubly-deranges' populations, across their $m! \times 2^m$ possible trajectories. The golden ratio is associated, in contrast, with growth balancing these extremes, EV-CF growth, and with squares. Also associated with squares is the assumption that $\frac{\partial C_m}{\partial F_{m,n}}$ is constant (i.e., a fixed hyperbole), Eq.(3a). It indicates that all factors are inserted into a common number of permutations (making all factors' diagonals the same size, and the population structure, overall, a 'square').

Unfounded (CF) Growth. What is the growth rate necessary to collect a square with m factors? We say $m - 1/m$ is the 'delay' for counterfactual observations in a $m \times m$ square. Any population a must wait $m - 1/m$ samples to complete a row [§](i.e., collect $b, c, d \dots [m]$). We then write $m - 1/m$ for the length of a 's balancing cycle, and $m + 1/m$ for its growth-balance cycle. The

[‡]the equation uses the Pythagorean theorem in reciprocal form, as it includes the triangle's altitude.

[§]where 1.0 is the cost to sample a new difference, with repetition.

growth-only cycle length is, consequently, their difference, $2/m$. We denote population sizes in each of these cycles: $n_{\bar{a}}$ (balance), n (balance-growth) and n_a (growth). Across time, these quantities express the added cost populations incur to collect, together, a balanced sample. Spatially, they indicate the spatial-level in which they become balanced. Consider the latter, where each location becomes a square cell. Population size n_t , with m factors balanced, follow the periodic difference equation $n_{t+m} = n + F_{m,t}$, or,

$$n_{t+m} = \sum_{n_t} \left[\frac{1}{n_t} \left(m + \frac{1}{m} \right) + n_t \left(m - \frac{1}{m} \right) \right], \quad \sum_{n_t} \frac{1}{n_t} \left(m + \frac{1}{m} \right) \rightarrow n, \quad \sum_{n_t} n_t \left(m - \frac{1}{m} \right) \rightarrow F_{m,t} = n_{\bar{a}},$$

(4a)
(4b)
(4c)

$$\frac{\partial n_{\bar{a}}}{\partial t} = 1.6180\dots (\phi), \quad (4d) \qquad \frac{\partial n_a}{\partial t} = 2, \quad (4e) \qquad \frac{\partial n_{\bar{a}}}{\partial n_a} = \frac{\phi}{2}, \quad (4f)$$

for a constant $m \ll n$. Eq.(4c) is an alternative expression for the Fibonacci series[¶] and, according to Eq.(4b), n is fixed per population, under growth with fixed bandwidth^{||}. This reproduces, alternatively, the rates in the previous section. In a random sample with treatment variable a , $\mathbb{E}[\frac{\partial n_a}{\partial t} | \mathbf{x}_0] = 2$, as, at each 2 time intervals, we are expected to rebalance (random variables are bold). It corresponds to Eq.(4a) when $m = 1$, n_{t+1} . A location with this property has one population, a , balanced, and common external factors, $x_0 = X - \{a\}$. We can alternatively say that $p(a|\bar{a}) = 0.5$, or, $a \perp (X - \{a\}) | \mathbf{x}_0$, which are typical non-confounding conditions. If units in the location share the same external factors, and have the same number of members with a as without a , then expected outcome differences between them correspond to a 's effect, conditional on the common variation. That is, $\mathbb{E}[\Delta y(a) | \mathbf{x}_0] = y(x_0 + \{a\}) - y(x_0 - \{a\})$. Selection mechanisms in such locations operate with fair estimates of a 's impact (albeit, with low EV). Common factor frequency guarantees no selection biases in 'treatment' assignment, and common external factors, no unobserved confounding. The latter is an instance of the common-cause rule^{23,24}. In a square, instead of a single factor, **all m factors are balanced simultaneously** ($m > 1$). While single-factor balance requires a binomial series, balancing several factors requires Fibonacci (i.e., square diagonal expansion). Each population, in this case, has asymptotic period $\mathbb{E}[\frac{\partial n_a}{\partial n_{\bar{a}}}] = \frac{2}{\phi}$ (twice the delay for each diagonal). Square accumulation, furthermore, increases the EV of all its populations simultaneously⁴, Fig.1(b, upper-right). A spatial square can thus be thought as accumulating higher-frequency local and mutual variation, while sharing the external, and slower, collectively¹¹. Squares are also a generalization of the Shapley value, the central Cooperative solution in Game-Theory. This suggests a hierarchical organization for systems in complex environments.

[¶] $F_{m,t+1} = F_{m,t-1} + F_{m,t} \times \left(m - \frac{1}{m} \right)$; $F_{m,0} = 0$, $F_{m,1} = 1$, see²².

^{||} $\sum_{n_t} \frac{1}{n_t} \left(m + \frac{1}{m} \right) = \frac{n_t \times m}{n_t} + \frac{n_t}{n_t \times m} = m + \frac{1}{m}$.

EV-CF Growth and Hyperbolic Geometry. Euler's required period²¹ to derange one population is $e = 2.7182\dots$. Substituting this in Eq.(4a)–(4c), for growth with unitary bandwidth,

$$\left(e + \frac{1}{e}\right) = \frac{\cosh(1)}{2}, \quad \left(e - \frac{1}{e}\right) = \frac{\sinh(1)}{2}, \quad \tanh(n) = \frac{\sinh(n)}{\cosh(n)} = \omega^{-1}, \quad (5a)$$

$$e^{\pm \operatorname{arctanh}\left(\frac{\partial D_n}{\partial F_{m,n}}\right)} = \frac{\left(1 \pm \frac{\partial D_n}{\partial F_{m,n}}\right)}{\sqrt{\left(1 - \frac{\partial D_n}{\partial F_{m,n}}\right)^2}}, \quad (5b) \quad \frac{\cosh(n)}{\partial n_a} \rightarrow 0.8090\dots \text{ (EV-CF)}, \quad (5c)$$

which suggests that hyperbolic functions can express population sizes in balance (\sinh) and growth-balance (\cosh) cycles, as well as the growth process' chosen trade-off between the two (\tanh). The same functions appeared in Eq.(2). The equations also suggest, from de Moivre's theorem, an interpretation of hyperbolic angles as the number of growth-balance cycles a system has undergone, $[\cosh(1) + \sinh(1)]^n = \cosh(n) + \sinh(n)$, and, from Euler's equation, the rate of a single cycle without balance, $e^{-1} = \cosh(1) - \sinh(1)$. Since $\cosh(n) = (1 - \tanh^2(n))^{-\frac{1}{2}}$, Eq.(3c) suggests expressing bandwidth in terms of $\tanh(n)$,**Eq.(5a). Since $\sinh'(n) = \cosh(n)$, Eq.(4f) indicates the per-population asymptotic rate in balanced growth, Eq.(5c). The hyperbole with this relative \cosh and \sinh growth rate is indicated in Fig.1(b).

Statistical Frame-of-Reference Invariance. While the concept of invariance (of a black-box estimator's response) has applications in Statistics and Machine Learning^{25,26}, the previous definition brings it closer to how it is understood in the Sciences. A full set of counterfactuals from a fixed reference x_0 constitute the set of all discrete differences $x - x_0$. Observation of complete counterfactual sets allow effect observations to become independent of the particular frame-of-reference in which those observations were made, increasing their EV. Multiple square accumulation constitutes a transition between two optimal non-parametric causal effect estimators, from homogeneous to heterogeneous populations⁴.

Eq.(3c) coincides with Lorentz factor γ^{27} . It is natural to think of the transformation as a hyperbolic rotation, as suggested by Emile Borel in 1914²⁸. Here, it preserves frequency relations among factors, $n_a/n_{\bar{a}}$, under changes of basis of the type $x=x_0+\{a\}$ and $x=x_0-\{a\}$. Increase of counterfactual observations at an EV level rotates populations in the hyperbolic plane across that level's hyperbole, which led to an interpretation of hyperbolic angles as growth progression with non-zero bandwidth, Fig.1(b). This interpretation also points to an alternative expression for exponential growth as a rotation γ with period $\frac{m}{2}$, Eq.(5b). Hyperbolic relations appear in (heterogeneous) systems where time-to-EV is long, Fig.1(b, upper-right).

**with $n = \operatorname{arctanh}(\omega^{-1}) = \operatorname{arctanh}\left(\frac{D_n}{F_{m,n}}\right)$, which, lets n be the number of accumulated derangements per fixed $F_{m,n}$ (i.e., per square).

Related Models. Exponential growth with limited capacity, described by sigmoid curves, are common models for growth across disciplines. A sigmoid is simply a rescaled tanh function²⁹, which is central here (*Sect. Heterogeneous Selection*, see also for the relation to Power-Laws). In such models, capacity is exogenous and unknown, while here it is an endogenous statistical limit ω . The human population, as well as past isolated populations, have hyperbolic forms³⁰. These are the global 'ends' of the nested spatial process proposed, with local populations expected to follow exponential-binomial growth. Brownian growth in changing environments^{31,32} follows populations' e -fold time (i.e., delay to derange). We formulated this as growth with unitary bandwidth, driven by randomness exclusively, and without a binomial balancing component. Hyperbolae are commonly assumed forms for demand-supply relationships, and starting-points of several Economical theories³³. The model justifies multiple empirical observations in the Economic Complexity literature, left unexplained by previous models, such as the nested, and triangular-matrix, distribution of occupations³⁴⁻³⁷, and multi-scale fitness periodicity across locations¹¹. All previous models make it difficult to model population diversity, which the current has as starting-point. From their formulation, it is difficult to understand what population structures they create¹⁵, and, as consequence, the long-term effects of their proposed parameters.

3 Results

Data used encompasses microdata of American decennial censuses from 1840 to 1940, and approximately 65 billion individual-level records. This non-aggregate data allows us to calculate pairwise factor differences for all individuals living in the Continental US. This, in turn, allow us to assemble squares across thousands of increasing spatial-levels. The time range corresponds to the highly tempestuous decades of American urbanization, incited by rapid industrial growth and immigration into cities. In 1840, only 10% of the American population was urban. By 1940, it already neared 60%. The data provides a unique view into the relationship among urban growth, spatial organization, and the incorporation of new industries and populations into cities.

We consider economic and demographic changes as we go from the individual, or household, spatial-level all the way to the national, throughout these years. We create increasing samples, containing sample units at arithmetically increasing levels, $s_{t+1}=s_t+\Delta s$ (starting from the local s_0). We repeat this for approximately 60K American locations, x_0 . Fig.2(b) illustrates this process. It shows two locations in New York city. At the city level, the two locations share a large amount of external variation (i.e., economic and demographic variations across the rest of the country). This transversal captures patterns of difference and overlaps, for all x_0 , as we increase scale.

Economic distribution across space can be described by the primary occupation and industry of each census individual. We discuss demographic (non-economic) variables in the Supplementary Material. Fig.2(c) illustrates empirical frequency for all occupations (each a curve) at 4 different spatial-levels, going from the local to the state level in Massachusetts (MA) and New York (NY), 1880. They were the country's economic centers until the beginning of the 19th century.

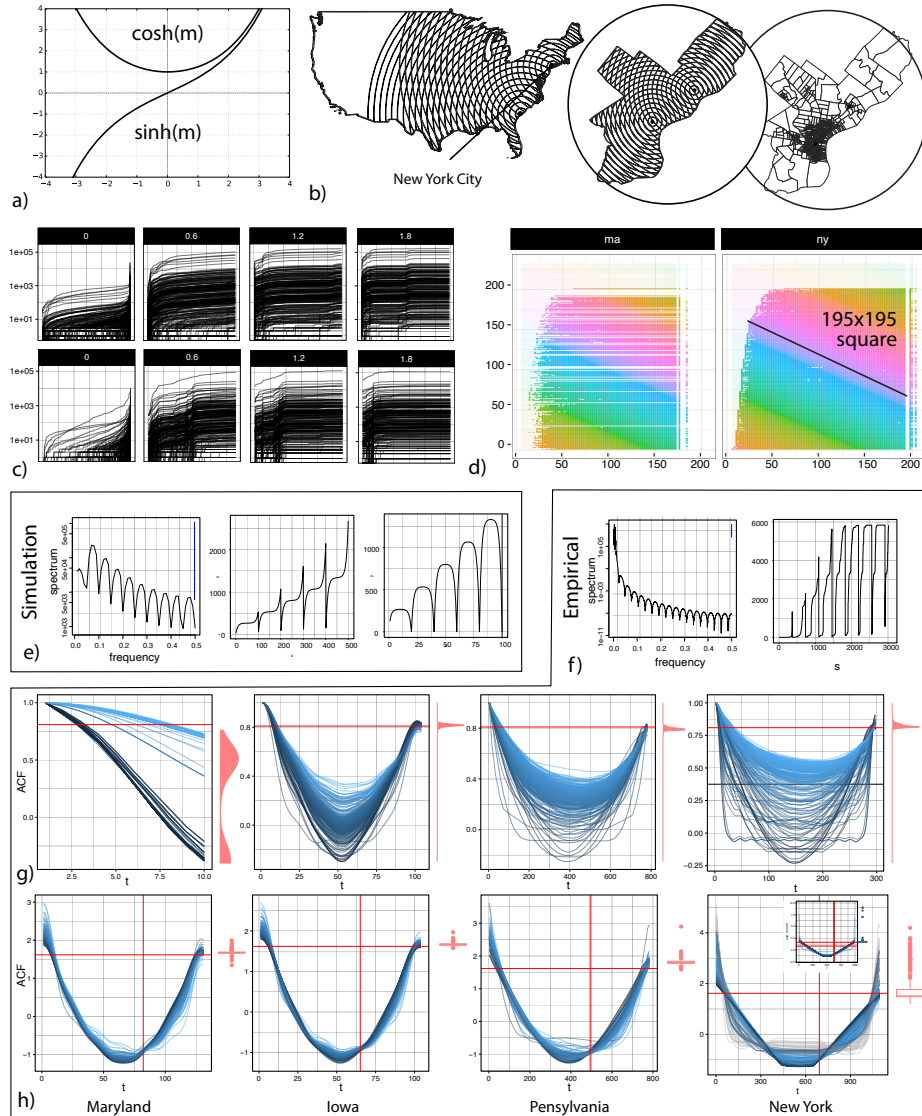


Figure 2: **(a)** \sinh and \cosh functions, **(b)** increasing spatial-levels starting at two example locations (national and city-levels), same-location pairs share external variation, we consider economic changes for $\sim 60K$ locations, under increasing scales, and the resulting population overlap and difference (correlation) patterns, finest spatial-level for New-York City (1880, right), **(c)** occupation frequency ranks vs. location across 4 example scales, each curve is one occupation, **(d)** enumerated Latin-Squares histograms for Massachusetts and New York, the latter has a square with almost all occupations, **(e)** periodogram of $\cosh(100) + \sinh(100)$, $\sinh(100)$ and $\cosh(100)$, **(f)** empirical per-occupation periodogram and frequency-ranked series in (c), **(g)** occupation auto-correlation vs. spatial-level in 1880, economically non-integrated locations have linear correlations, integrated locations have catenaries (free-hanging rope), with given length, for each occupation, $y=1.0$ indicate complete correlation with the local level, probability distribution of their slack (red, sidepanel) indicate a fixed \cosh increase per factor at 0.81 (red horiz. line), across all occupations and locations, Eq.(5c), **(h)** standardized catenary across *all* years, boxplots (red, sidepanel) show slack invariance for all occupations, locations and years, and constant ratio between \sinh and \cosh growth, $m \times (1 - \frac{1}{e})$ (red vert. line) is a fixed point in binomial-exponential (EV-CF) to exponential (EV) rate transitions.

The distribution has the familiar shape of a wave that moves to the left. New York reaches a stationary shape at a lower level s_{sq} (2nd upper panel, 0.6 lat-lon distance). We demonstrate these correspond to levels where squares are completed across factors. All squares in a location can be enumerated through an expensive computational procedure⁴. Histograms are shown in Fig.2(d), where each color correspond to one of 220 occupation classifications. We see NY has a spatial square that extends to almost all occupations, while MA has missing occupations (horizontal gaps) in comparison.

3.0.1 The Hanging-Rope Model of Unbiased Growth

The Catenary is a curve with long scientific history, being first formulated by Galileo Galilei. Unlike circles and geodesics, they are sums of exponentials. They provide a convenient way to visualize the previous model, since their equation in (x, y) Cartesian coordinates is $y = h \cosh\left(\frac{x}{h}\right)$, and length $h \sinh\left(\frac{x}{h}\right)$. They describe a free-hanging rope, whose 'slack' h is the difference in height, y , between its two hanging points³⁸.

Fig.2(a,e) depicts general shapes for functions $\cosh(n)$ and $\sinh(n)$, and for the spectrum of $\cosh(n) + \sinh(n)$. Fig.2(f) illustrates the *empirical* spectrum of curves in Fig.2(c). Taking square sizes m to be temporal or spatial coordinates leads to specific temporal or spatial correlation patterns⁴ across scales. Fig.2(g) shows sample Autocovariance Function (ACF) across 5000 spatial-levels from the local to the national level (as those illustrated in Fig.2(c)). It demonstrates that the auto-correlation of each occupation, as we increase spatial-levels, trace catenaries. The horizontal line $y = 1.0$, of unitary correlation, is associated with the limit $F_{m,n} = 0$ where, despite the increasing scale, there are no added population differences. Each catenary is a set of points with constant ratio $C_m/F_{m,n}$, which is **the defining property of squares**, Eq.(3a).

Fig.2(g) illustrates 4 typical cases among states: rural (Maryland, similar are Rhode Island, Louisiana, Arizona, Idaho, Wyoming, etc.), rural and complex (Iowa, Ohio, Wisconsin, Colorado, etc.), urbanizing and complex (Philadelphia, Massachusetts, Indiana, Michigan, New Jersey, etc.), and metropolitan (New York). Plots for all other states, and for other variables, are available in the Supplementary Material. The first group have linear decreases in correlation, as expected in non-interdependent systems. From 1840, the USA economy and cities become increasingly interdependent. After 1900, no longer any state had such linear correlation signatures. Periodic and linear (zig-zag) correlations, with period $m/2$, are related to non-increasing EV, Fig.1(b). Purely periodic, without growth, and exponential correlations correspond to catenaries with $h = 0$ (where a system returns to its original state after a lag). Standardizing catenaries³⁸ make h indicate relative growth rate, $h = \cosh(m) - \cosh(0)$.

Fig.2(h) shows standardized catenaries for all years and locations. It indicates that cosh per factor remains constant across a wide range of levels, up to s_{sq} , and starting at the local. This was

anticipated by Eq.(5c). The rate up to s_{sq} is 0.81% of correlation. Box-plot for h , across all levels, years, occupations, and locations, are shown in Fig.2(h, sidepanel, red). For all spatial-levels below s_{sq} , factors a and \bar{a} remain balanced, with binary-exponential rates (i.e., hyperbolic functions with period $m/2$). Levels above s_{sq} reverse to exponential growth. We called this a transition between EV and EV-CF growth. This is indicated in plots by the dislocation of the catenary center, after s_{sq} , from $m/2$ to m/e . This is most apparent in urbanizing locations (Philadelphia and New York). Estimated levels s_{sq} for all states are shown in Fig.3(d). New York is the only state, at the studied period, with 2-level squares. Catenaries for the lower square are shown in Fig.2(h, upright-panel), and levels are illustrated cartographically in Fig.3(b). The two squares' factors are disjoint (gray, lower factors taking exponential rates in higher). American states had then different work forces, economic characteristics, and regional distributions. While catenary lengths are different across occupations and locations, Fig.2(g), their slack remains invariant across all occupations, locations and years, Fig.2(h).

3.0.2 Heterogeneous Selection

Zipf's law was originally formulated to describe word frequency in corpora. It started much of the recent scientific interest in Power-laws, with famous explanations such as the principle-of-least-effort and preferential-attachment^{7,39,40}. It is the central model for city size distribution^{5,7}. The law is based on a frequency ranking of the studied factors, and thus, on only one of all their permutations. It is, here, associated with a homogeneous, or 'winner-takes-all', conception of selection.

Fig.3(a) depicts general shapes for curves $\tanh(n)$ and $\coth(n)$. Fig.3(g) shows occupations' frequency ranks across locations for increasing spatial-levels. Each curve is one level. An occupation's minimum rank across all locations is denoted r_0 (green), and its maximum rank r_ω (red). The maximum-frequency rankings (red) are closely related (*Methods*) to Zipf's frequency rankings and the Pareto distribution, as the three are Power-laws. With a homogeneous selection assumption, we expect one highest-rank industry ('winner') across locations, and thus $r_\omega - r_0 = 1$. What we observe, however, is that factors are ranked in constant-sized ranges, as visualized by squares. Each occupation is the highest ranked in *some* location, the second in other, etc. These rankings define an arithmetic series - $r_0, r_0 + 1, r_0 + 2, \dots, r_\omega$ - for each location. The series has mean $\bar{r} = \frac{r_0 + r_\omega}{2}$, which is also shown (blue). The previous model predicts that $r_\omega - r_0$ is constant, and reflect the bandwidth $\omega = \tanh(n)^{-1}$. Fig.3(g) shows that empirical rankings have a fixed $r_\omega - r_0$, with increasing minimum r_0 and fixed point in $(m/2, m/e)$. Squares correspond to the band indicated in Fig.3(c, gray). The square rotates around $(m/e, m/2)$ by some angle $\theta_1 \approx \arctan(r_\omega/r_0)$. A closer examination of both branches (red and green) reveals they correspond to the positive and negative sections of the $\coth(n) = 1/\tanh(n)$ function, Fig.3(h,a).

Imagine the following process: pick a location x_0 , and its most and least-frequent factors

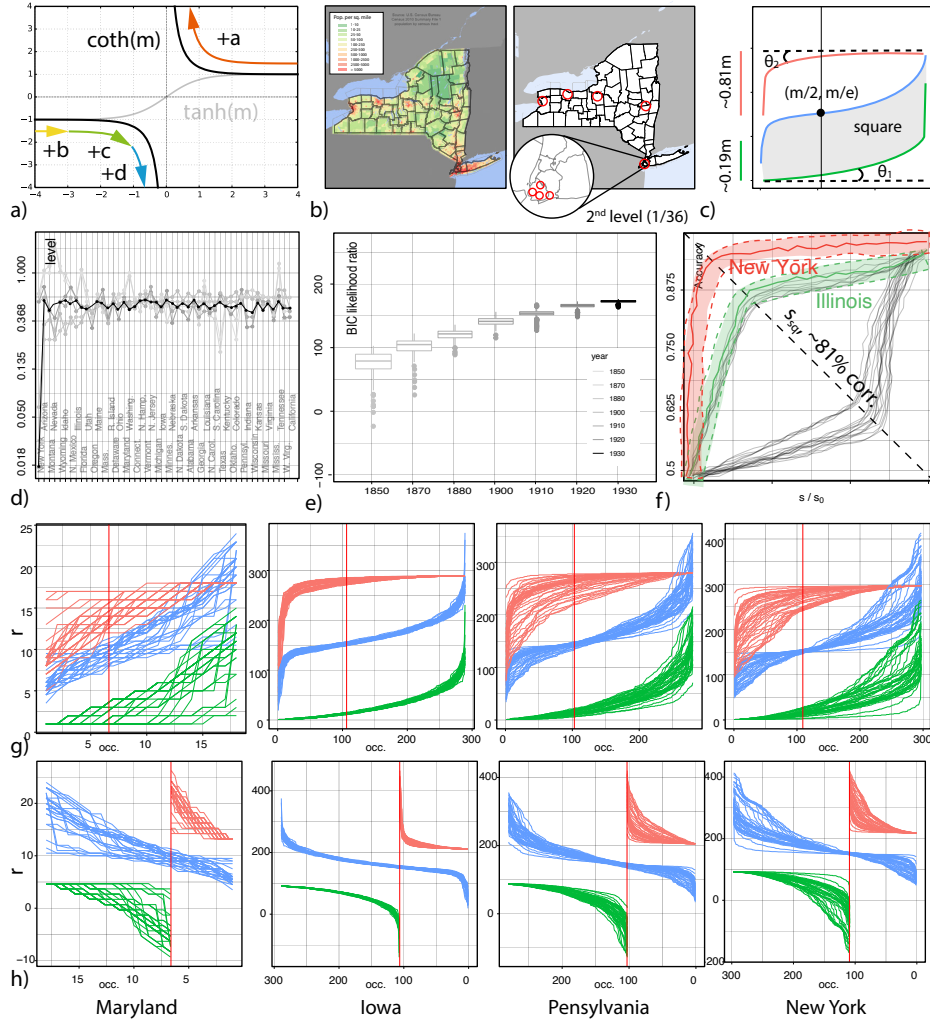


Figure 3: **(a)** \coth and \tanh functions, colored arrows illustrate square factor frequency increases with scale, a (red) is the location's most frequent factor, b, c, d, \dots are most-frequent factors in other locations, **(b)** New York (NY) state population density (left), NY has squares at two levels s_{sq} after 1910, at 0.018 and 0.65 lat-lon distance (red circles), **(c)** schematic depiction of frequency rank vs. spatial-scale plots in (g), area between min. (green) and max. (red) ranks across all locations indicate square size (gray), **(d)** s_{sq} (spatial-level of first square) for all states and years, levels s_{sq} become less random, and more similar, with increasing economic integration, **(e)** BIC model likelihood ratio of \coth over a Zipf model, Zipf uses only one (frequency-based) permutation, it becomes increasingly inaccurate as locations become more complex (and squares larger), **(f)** accuracy of state-of-the-art predictors vs. spatial-level, s_{sq} level is diagonal (dashed), NY (red) gains little from external data, as it already encompasses large amounts of variation (bandwidth), other locations gain significantly from others' data as they have **incomplete squares**, **(g)** max. (red) and min. (green) frequency ranks across locations, each curve is a different spatial-scale, blue curves indicate square size, which follows a \tanh function, $(m/2, m/e)$ inflection (red vert. line), **(h)** \coth model, as illustrated in (a), with empirical data.

(i.e., with rank 1 and m). Label them, respectively, a and z_0 . Balance z_0 to match a 's frequency. Move one spatial-level up, pick a second least-frequent factor (label it z_1), balance, and repeat. In a single square row, n_a is the number of units in cell a , and $n_{\bar{a}}$ in all others cells (i.e., not a). The cost to balance each z is thus n_a/ω . So, we can write, for all locations x_0 , and levels $s_0 \leq s \leq s_{sq}$,

$$\begin{aligned} n_a \times \frac{1}{\omega} - n_{z \in \bar{a}} &= 0, \\ n_a - n_{z \in \bar{a}} \times \coth(n) &= 0, \end{aligned} \tag{6}$$

which implies $\sum_{i=0}^{sq} n_{z_i} = n_{\bar{a}}$, and $n_a = n_{\bar{a}}$. Observed min. and max. ranks take this shape across spatial-levels, Fig.3(g,h). The *coth* function separates, by sign, each location's balancing and growth phases, and reveals the order in which squares are completed in real systems, Fig.3(a). This is illustrated as one hyperbolic rotation, with subsequent square derangements leading to others. This reflects the spatial transversal used (bottom-up), where, until level s_{sq} , each location corresponds to a square row. The process also constitutes a change of perspective, from selection as winner-takes-all processes to ω -winners-take-all (driven by changing, but shared and stationary, external conditions).

Methodologically, this suggests fitting a *coth* function to observed frequency ranks. A Zipf-distribution can be fit by Power-law or Pareto distribution regressions. We show in the Supplemental Material that the Pareto distribution can be used to reproduce, with alternative methods, the results in Fig.2(g,h). The 81%–19% split is apparent in the previous plots, as the ratio between positive and negative *coth* branches' angles, Fig.3(c). Bandwidth increases imply increasingly different min. and max-frequency permutations. This predicts that Zipf-Pareto regressions will become, as cities become more heterogeneous, increasingly inaccurate (compared to *coth*). This is illustrated in Fig.3(e), which shows increase of up to 18 times fit likelihood favoring the *coth* model throughout the studied period, according to a Bayesian Information Criterion (*Methods*).

What impact does complete squares have in their populations statistically (in respect to the EV and CF of effects)? This has been formulated theoretically, and demonstrated practically in simulated, cohort, experimental, economic, and genetic data^{4,11,41}. Fig.3(f) demonstrates a further result, using census microdata, with an Accuracy vs. Spatial-level plot. It shows the maximum accuracy of 24 state-of-the-art supervised algorithms predicting whether a given occupation will grow, or not, in a location, as we use data from increasing spatial-levels (starting at the local and reaching all national data). According to Fig.2(h), spatial-level s_{sq} concentrates around an 81% oversample for a local subset of occupations, across locations. According to Fig.3(d), these levels become increasingly similar with time, across locations. In Fig.3(f), s_{sq} is mapped to the diagonal (dashed). Each state is one curve. Bootstrap accuracy variation bands (across states' locations) are shown for the two most accurate states, New York (red) and Illinois (green). We observe that New York gains little from external data (above s_{sq}) as it already contains, within its boundaries,

high levels of variation. Homogeneous locations, in contrast, have incomplete squares, and observed effects are susceptible to external and unobserved variation. This also implies that, without unobservables, $\sim 81\%$ of the sample is sufficient for prediction. The impact of unobservables is formulated in ⁴. This demonstrates an information asymmetry among locations (where the former is more useful to the latter than vice-versa). Network and Economic Development studies often describe New York as an early 'information hub' or 'sandbox for innovation'. The previous substantiate, statistically, these descriptions.

4 Conclusion

The challenge for any adaptive system in a complex environment is how to organize its under-control variation in face of its external. There is a cooperative dimension to this problem, where systems with common external variation (e.g., that are in the same location) can increase both the external validity and unbiasedness of their strategic choices by coordination. Each collected square increases, simultaneously, the external validity of ω , fully unconfounded, populations. The set of all squares is related both to an optimal estimator in Theoretical Statistics and a solution in Cooperative Game-Theory. It is, however, not only this asymptotic state that is optimal, but the way there (i.e., the growth process), given its limits. Throughout growth, ω populations remain fully unconfounded, with effects increasingly externally valid. Exponential growth and hyperbolic functions offered a natural implementation and visualization for these alternative growth patterns.

Increase in external validity, for $\omega = 1$, requires exponential growth. Increase in unconfoundness requires, however, Fibonacci, with a half-golden growth ratio. The latter increases in 81% the required population size for each individual population, and should be a requirement of large selection systems. The consequent 80-20 split is employed everyday across real-world systems, and in Machine Learning practice. We demonstrated not only functional-form evidence for the model, as typical^{5,7}, but also enumerative, combinatorial, and for its 3 predicted growth rates. Most uniquely, we connected growth to the statistical environment (biases, predictability and explainability) growth processes create for their populations. These contributions predicted, and confirmed, Golden rates for city growth, and offered an explanation for the Pareto principle.

References

1. Cooter, R. & Parisi, F. *Foundations of law and economics* (Edward Elgar, Cheltenham, UK; Northampton, MA :, 2009).
2. Newman, M. Power laws, pareto distributions and zipf's law. *Contemporary Physics* **46**, 323–351 (2005). URL <https://doi.org/10.1080/00107510500052444>.
3. Holden, K., Butler, J., Elam, K. & Lidwell, W. *Universal principles of design* (Rockport Publishers, Beverly, Mass., 2010).

4. Ribeiro, A. F. & Nonato, L. G. The external validity of combinatorial samples and populations. (*Journal version, Under Review, Supporting Material*) (2021).
5. Gabaix, X. Zipf's law for cities: An explanation. *The Quarterly journal of economics* **114**, 739–767 (1999).
6. KORTUM, S. S. Research, patenting, and technological change. *Econometrica* **65**, 1389–1419 (1997).
7. Verbavatz, V. & Barthelemy, M. The growth equation of cities. *Nature* **587**, 397–401 (2020). URL <https://doi.org/10.1038/s41586-020-2900-x>.
8. Li, R. *et al.* Simple spatial scaling rules behind complex cities. *Nature Communications* **8**, 1841 (2017). URL <https://doi.org/10.1038/s41467-017-01882-w>.
9. Song, C., Qu, Z., Blumm, N. & Barabási, A.-L. Limits of predictability in human mobility. *Science (American Association for the Advancement of Science)* **327**, 1018–1021 (2010).
10. Bettencourt, L. M. A. & Zünd, D. Demography and the emergence of universal patterns in urban systems. *Nature Communications* **11**, 4584 (2020). URL <https://doi.org/10.1038/s41467-020-18205-1>.
11. Ribeiro, A. F. Competition, diversity and quality. *Physica A* **568**, 125683 (2021).
12. Weitzman, M. L. Recombinant growth. *Quarterly Journal of Economics* **113**, 331–360 (1998). URL <https://doi.org/10.1162/003355398555595>.
13. Uzzi, B., Mukherjee, S., Stringer, M. & Jones, B. Atypical combinations and scientific impact. *Science (American Association for the Advancement of Science)* **342**, 468–472 (2013).
14. Xie, Y. Population heterogeneity and causal inference. *Proceedings of the National Academy of Sciences* **110**, 6262 (2013).
15. Allen, B. *et al.* Evolutionary dynamics on any population structure. *Nature (London)* **544**, 227–230 (2017).
16. Lieberman, E., Hauert, C. & Nowak, M. A. Evolutionary dynamics on graphs. *Nature* **433**, 312 (2005).
17. Gao, J., Barzel, B. & Barabási, A.-L. Universal resilience patterns in complex networks. *Nature (London)* **530**, 307–312 (2016).
18. Walliser, B. Learning versus evolution: From biology to game theory. *Biological Theory* **6**, 311–319 (2011). URL <https://doi.org/10.1007/s13752-012-0071-1>.
19. Taylor, P. D. & Jonker, L. B. Evolutionary stable strategies and game dynamics. *Mathematical biosciences* **40**, 145–156 (1978).

20. Lee, A. J. *U-statistics : theory and practice* (M. Dekker, New York, 1990).
21. Sandifer, C. E. *How Euler did it (Chapter 17, pg.103)*. The MAA tercentenary Euler celebration ; v.3 (Mathematical Association of America, Washington, DC], 2007).
22. Gazale, M. J. *Gnomon: from pharaohs to fractals* (Princeton University Press, Princeton, N.J, 1999).
23. Reichenbach, H. *The direction of time*, (University of California Press, Berkeley, 1956).
24. Scholkopf, B. *et al.* Toward causal representation learning. *Proceedings of the IEEE* **109**, 612–634 (2021).
25. Buehlmann, P. Invariance, causality and robustness. *Statistical science* **35**, 404–426 (2020).
26. Peters, J., Bühlmann, P. & Meinshausen, N. Causal inference by using invariant prediction: identification and confidence intervals. *Journal of the Royal Statistical Society. Series B, Statistical methodology* **78**, 947–1012 (2016).
27. Hucks, J. Hyperbolic complex structures in physics. *Journal of mathematical physics* **34**, 5986–6008 (1993).
28. Borel, E. *Introduction geometrique a quelques theories physiques* (Paris, 1914).
29. LeCun, Y. A., Bottou, L., Orr, G. B. & Müller, K.-R. *Efficient BackProp*, 9–48 (Springer Berlin Heidelberg, Berlin, Heidelberg).
30. Banks, R. B. *Growth and Diffusion Phenomena: Mathematical Frameworks and Applications*, vol. 14 (Springer Berlin / Heidelberg, Berlin, Heidelberg, 1994).
31. Taylor, G. I. Diffusion by continuous movements. *Proceedings of the London Mathematical Society* **s2-20**, 196–212 (1922).
32. BRETHERTON, C. S., WIDMANN, M., DYMNIKOV, V. P., WALLACE, J. M. & BLADE, I. The effective number of spatial degrees of freedom of a time-varying field. *Journal of climate* **12**, 1990–2009 (1999).
33. Humphrey, T. M. The early history of the box diagram. *Economic quarterly* **82**, 37 (1996).
34. Leontief, W. *The structure of the U.S. economy* (W.H. Freeman, San Francisco, 1965).
35. SAAVEDRA, S., REED-TSOCHAS, F. & UZZI, B. A simple model of bipartite cooperation for ecological and organizational networks. *Nature (London)* **457**, 463–466 (2009).
36. Bustos, S., Gomez, C., Hausmann, R. & Hidalgo, C. A. The dynamics of nestedness predicts the evolution of industrial ecosystems. *PloS one* **7**, e49393–e49393 (2012).
37. Balland, P. A. *et al.* Complex economic activities concentrate in large cities. *Nature human behaviour* **4**, 248–254 (2020).

38. Cella, P. Reexamining the catenary. *The College mathematics journal* **30**, 391–393 (1999).
39. Tria, F., Loreto, V., Servedio, V. D. P. & Strogatz, S. H. The dynamics of correlated novelties. *Scientific reports* **4**, 5890–5890 (2014).
40. Adamic, L. Unzipping zipf’s law. *Nature* **474**, 164–165 (2011). URL <https://doi.org/10.1038/474164a>.
41. Ribeiro, A. F. An experimental-design perspective on population genetic variation (2021). 2108.06580.